Physical properties of hematite α-Fe_2O_3 thin films: application to photoelectrochemical solar cells

S. S. Shinde, R. A. Bansode, C. H. Bhosale, and K. Y. Rajpure†

Electrochemical Materials Laboratory, Department of Physics, Shivaji University, Kolhapur 416004, India

Abstract: The physical properties and photoelectrochemical characterization of aluminium doped hematite α-Fe_2O_3, synthesized by spray pyrolysis, have been investigated in regard to solar energy conversion. Stable Al-doped iron (III) oxide thin films synthesized by a spray pyrolysis technique reveals an oxygen deficiency, and the oxide exhibits n-type conductivity confirmed by anodic photocurrent generation. The preparative parameters have been optimized to obtain good quality thin films which are uniform and well adherent to the substrate. The deposited iron oxide thin films show the single hematite phase with polycrystalline rhombohedral crystal structure with crystallite size 20–40 nm. Optical analysis enabled to point out the increase in direct band-gap energy from 2.2 to 2.25 eV with doping concentration which is attributed to a blue shift. The dielectric constant and dielectric loss are studied as a function of frequency. To understand the conduction mechanism in the films, AC conductivity is measured. The conduction occurs by small polaron hopping through mixed valences $Fe^{2+/3+}$ with an electron mobility 300 K of 1.08 $cm^2/(V{\cdot}s)$. The α-Fe_2O_3 exhibits long term chemical stability in neutral solution and has been characterized photoelectrochemically to assess its activity as a photoanode for various electrolytes using white light to obtain I–V characteristics. The Al-doped hematite exhibited a higher photocurrent response when compared with undoped films achieving a power conversion efficiency of 2.37% at 10 at% Al:Fe_2O_3 thin films along with fill factor 0.38 in NaOH electrolyte. The flat band potential V_{fb} (–0.87 V_{SCE}) is determined by extrapolating the linear part to $C^{-2} = 0$ and the slope of the Mott-Schottky plot.

Key words: photoelectrochemical; hematite; spray; photoanode

DOI: 10.1088/1674-4926/32/1/013001 **EEACC:** 2520

1. Introduction

With the advent of nanotechnology, there has been a resurgence of interest in metal oxides as suitable candidates for photoelectrochemical (PEC) studies. Binary oxides M_2O_3, where M is a trivalent metal, crystallize in the corundum structure and occur in n- as well as p-types[1]. In this category, the hematite α-Fe_2O_3 was selected as a prototype due to its technological use as a catalyst[2, 3] and photocatalyst[4]. Moreover, it has found increasing application because of its dielectric properties and its breakthrough having unexpectedly large thermopower. The hematite is predicted to be an insulator with a localized Fe^{3+}:3d electron[5]. However, a slight deviation from the stoichiometry induces an enhancement of the electrical properties allowing photoelectrochemical (PEC) characterization. On the other hand, there is an increasing interest in the photoactive functional oxide materials. As one of the main fields of solar energy research concerns the development of so-called solar fuels[6] and considerable attention has been focused on developing new semiconductors (SC) for the PEC conversion[7, 8]. Practical advantages pertinent to solar energy were reported previously[9]. Fe_2O_3 has a gap E_g which averages 2 eV, absorbing ~40% of the sunlight. Additionally, it is low cost, non-toxic and exhibits a chemical stability over a broad pH range[10]; these characteristics make it attractive for photocatalytic applications. The crystal lattice contains octahedral FeO_6 units, which determine that both the valence band (VB) and the conduction band (CB) are associated with the same cation, namely Fe^{3+}. Hence, VB is pH independent and for a given pH can be appropriately positioned with respect to the O_2/H_2O redox level in solution. However, whereas the physical properties of the hematite have been investigated[11, 12], the transport properties so far reported have been limited to the electrical conductivity, although some papers were devoted to the PEC characterization[13, 14]. Shwarsctein *et al*.[15] studied the substitutional doping to improve the electronic properties of α-Fe_2O_3 for solar photoelectrochemical (PEC) applications. However, we found that the introduction of strain in the lattice, which is achieved by isovalent substitutional doping of Al, can also improve the electronic properties. The results indicate that the incident photon conversion efficiency (IPCE) for 0.45 at % Al substitution increases by 2- to 3-fold over undoped samples. The α-Fe_2O_3 thin film photoanodes for solar water splitting were prepared by spray pyrolysis of $Fe(AcAc)_3$ studied by Liang *et al*.[16]. The donor density in the Fe_2O_3 films could be tuned between 10^{17} and 10^{20} cm^{-3} by doping with silicon. The highest photoresponse is obtained for Fe_2O_3 doped with 0.2% Si, resulting in a photocurrent of 0.37 mA/cm^2 at 1.23VRHE in a 1.0 M KOH solution under 80 mW/cm^2 AM 1.5 illumination.

An important feature of photovoltaic solar cells and of diverse optoelectronic devices studied in semiconductor physics concerns their current–voltage characteristics. The main requirements for suitable semiconductor photoelectrodes are (1) sufficient (sun) light absorption, (2) high chemical stability, (3) favourable energetic positions of the band edges with respect to the oxidation potential, (4) fast transport of photo-

† Corresponding author. Email: rajpure@yahoo.com
Received 20 July 2010

generated charge carriers, and (5) low cost. While the various preparation methods, such as chemical vapour deposition (CVD)[17], MOCVD[18], reactive ion beam sputtering[19] and laser-assisted CVD[20], result in excellent quality thin films, they lack flexibility and cost effectiveness. Therefore, it is of interest to study the PEC properties of α-Fe_2O_3, elaborated by a chemical route. In this paper, we report promising aluminium doped hematite α-Fe_2O_3 films with great reproducibility and homogeneous structure, deposited by conventional spray pyrolysis. Also, we have studied the room temperature dielectric measurements, including dielectric constant, dielectric loss and AC conductivity with frequency. In addition, the critical parameters in photoelectrochemical properties for hematite films obtained by spray are investigated and discussed. The entire data give new insight into the energetics of thin film systems of ionic compound materials.

2. Experimental

Undoped and aluminium doped hematite α-Fe_2O_3 thin films were deposited onto ultrasonically cleaned glass and fluorine doped tin oxide (FTO) coated glass substrates (having resistance 10–15 $\Omega/\square$) using a chemical spray pyrolysis technique. The high purity reagents in the deposition method involved the decomposition of an aqueous solution of high purity 0.1 M ferric trichloride (99.99%, A.R. grade, Aldrich) using double distilled water as a solvent. To achieve aluminium doping, aluminium nitrate was incorporated into the solution. The [Al]/[Fe] ratios calculated on at%, used in the starting solution, were 5%, 10%, 15%, 20%. The resulting solution was sprayed onto the preheated substrates held at an optimized substrate temperature of 623 K with compressed air as a carrier gas. Other preparative parameters were spray rate: 5 cc/min; nozzle to substrate distance: 33 cm; and nozzle diameter: 0.05 cm, kept constant for all experiments.

The structural characterization of deposited thin films was carried out by analyzing the X-ray diffraction patterns obtained using CuKα (λ = 1.5406 Å) radiation from a Philips X-ray diffractometer model PW-3710 and surface morphology was studied using a JEOL JSM-6360 scanning electron microscope (SEM). Absorption spectra were recorded at room temperature and near to normal incidence using a Systronic model 119. The AC parameters, such as capacitance (C) and dissipation factor ($\tan\delta$), of the films were measured in the frequency range 20 Hz to 1 MHz using an LCR meter (HP 4284A). The dielectric constant (ε') was calculated using the relation

$$\varepsilon' = \frac{C_{\rm p} t}{\varepsilon_0 A}, \tag{1}$$

where $C_{\rm p}$ is the capacitance of the film, t the thickness of the film, A the cross-sectional area of the film, and ε_0 the permittivity of free space (8.854×10^{-12} F/m). The AC conductivity of the films was estimated from the dielectric parameters. As long as the pure charge transport mechanism is the major contributor to the loss mechanisms, the AC conductivity ($\sigma_{\rm AC}$) may be calculated using the relation

$$\sigma_{\rm AC} = \omega\varepsilon'\varepsilon_0 \tan\delta, \tag{2}$$

where ω is the angular frequency and $\tan\delta$ the dissipation factor.

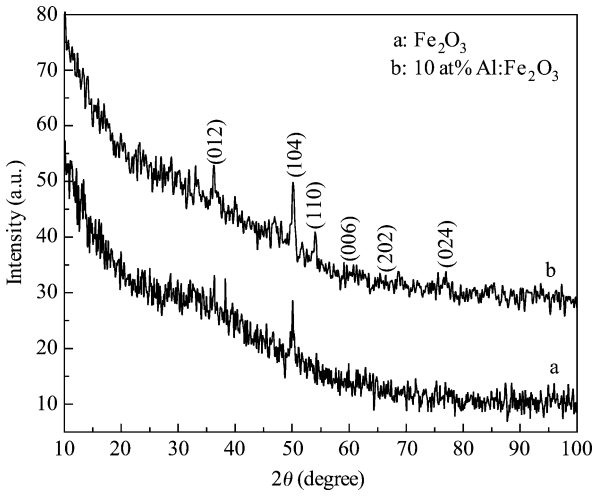

Fig. 1. X-ray diffraction pattern of pure and typical 10 at% Al: Fe_2O_3 (AFO) thin films deposited at a 623 K substrate temperature .

The photoelectrochemical study was performed in a conventional three electrode configuration, with the deposited thin film on fluorine doped tin oxide (FTO) coated glass as the working electrode (comprising modified n-undoped and doped iron oxide thin film as a photoanode), graphite as a counter electrode and SCE as a reference electrode. These three electrodes were fitted in the bakelite holder having thickness 1 cm and diameter 3.5 cm and fixed in a cylindrical corning glass cell with capacity 30 cm^3. The distance between the photoelectrode and the counter electrode was 0.5 cm and the exposed area to visible light was 1 cm^2. The photoelectrochemical (PEC) characteristics were measured for various electrolytes, such as KOH, KI, NaOH and Na_2SO_4 (0.1 M concentration of each electrolyte). For the measurement of power output characteristics, a two electrode configuration consisting of electrodes as a photo-anode and graphite as the counter electrode was used. Measurements for the power output characteristics and the current–voltage (I–V) characteristics in the dark and under illumination were studied at fixed intervals after waiting for sufficient time to equilibrate the system under forward and reverse bias conditions. Capacitance–voltage (C–V) measurements were carried out in the dark using an LCR bridge (Aplab model 4912) at a built in frequency of 100 Hz.

3. Results and discussion

3.1. Structural analysis

Figure 1 shows X-ray diffraction patterns of the undoped and optimized 10 at% Al doped iron oxide thin films. From these patterns it is clear that all of the synthesized films of α-Fe_2O_3 have a single phase. The films are nanocrystalline, polycrystalline and fit well with the rhombohedral crystal structure having space group R3 (148). These films of α-Fe_2O_3 are in correspondence with 24-0072 in a powder diffraction file (PDF) collected by the Joint Committee on Powder Diffraction Standards (JCPDS). The lower peak intensities are attributed to the lower film thickness (~115–135 nm) and the formation of an amorphous plus nanocrystalline phase in thin films. A slight hump in the XRD pattern around 32.19° is the evi-

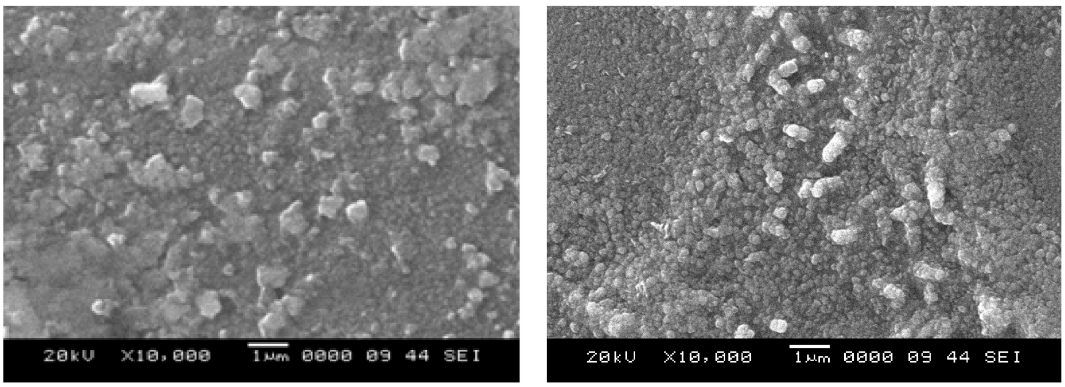

(a) (b)

Fig. 2. Scanning electron micrographs of (a) undoped and (b) 10 at% AFO thin films.

dence for this. For the 10 at% Al:Fe_2O_3 film, the diffraction angle of the (104) peak is almost in agreement with the Fe_2O_3 bulk single crystal, implying that no evident residual stress or inclusion-induced lattice distortion has developed in the Fe_2O_3 film due to Al incorporation. Some weak reflections, such as (012), (110), (006), (024) and (202), have also been observed but with small intensities. With relatively smaller peak intensities, this indicates that the point/cluster defects are produced, causing a certain amount of amorphization in the material.

The lattice parameters a and c of prepared α-Fe_2O_3 films are determined from the analysis of the X-ray diffraction patterns and are estimated from the formula of a rhombohedral system,

$$\frac{1}{d^2} = \frac{\left(h^2 + k^2 + l^2\right)\sin 2\alpha + 2\left(\cos 2\alpha - \cos\alpha\right)}{a^2\left(1 - 3\cos 2\alpha + 2\cos 3\alpha\right)}, \quad (3)$$

where α is the angle between to faces.

The calculated values of a and c for α-Fe_2O_3 films are a = 5.036 Å and c = 13.7460 Å, which are close to the values given in the above mentioned JCPDS card, a = 5.038 Å and c = 13.77 Å. The average particle size is calculated employing Scherrer's equation,

$$D = \frac{0.9\lambda}{\beta\cos\theta}, \quad (4)$$

where D is crystallite size, λ is wavelength of X-ray, β is full width at half maximum in radian, and θ is Bragg angle. The average crystallite size is found to be of the order of 39 and 21 nm for undoped and 10 at% Al:Fe_2O_3 thin films, respectively, so it plays an important role in photoelectrochemical performance. This effect can be explained if it is considered that (1) aluminium atoms do not substitute iron atoms, instead they occupy interstitial sites resulting in a large number of dislocations; and (2) probable formation of compound which is growing along with Al:Fe_2O_3. It might be possible because the ionic radii of aluminium (0.53 Å) are comparable with iron (0.62 Å) but far less than oxygen (1.4 Å).

3.2. Morphological behavior

Figure 2(a) shows the morphology of undoped α-Fe_2O_3 thin film. The micrograph depicts the polycrystalline nature of the film with random distribution of grains with varying sizes. Figure 2(b) shows the typical micrograph of 10 at% Al:Fe_2O_3 thin film. Doping induces the clustering of well established randomly oriented nanorods having an average diameter about ~170 nm and shows compact, homogenous and well adherent growth onto the substrate. It is believed that the extent of agglomeration of the particles with rods increases and thereby results in densification till pertaining some porosity with inter-cluster voids.

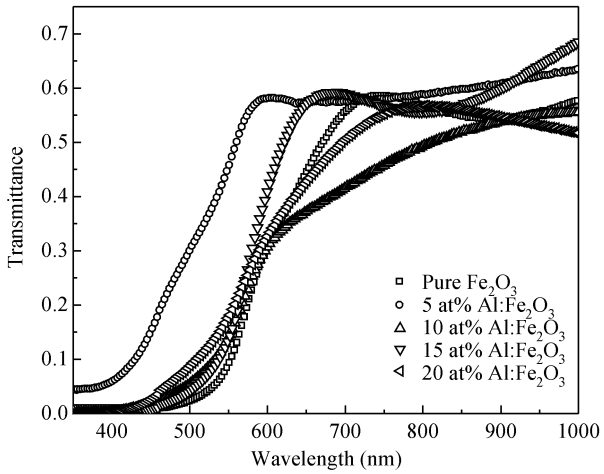

Fig. 3. Variation in specular optical transmittance against wavelength for pure and doped iron oxide thin films.

3.3. Optical properties

Figure 3 depicts the specular measurement of optical transmission spectra of pure and doped Fe_2O_3 in the wavelength range of 400–1000 nm at normal incidence. The transmission spectrum approaches semiconductor behavior with the appearance of interference maxima. The spectra display pronounced interference oscillations, as expected from the magnitudes of thickness and refractive index of the films. The data for the crystalline materials show peculiar characteristics that we will attribute to inhomogeneities in the film. At $\lambda < 606$ nm, the interference fringes become less pronounced due to the onset of absorption. The absorption can be caused by localized states between the conduction band and the Fermi level, and that ef-

Table 1. Various parameters of spray deposited pure and Al doped iron oxide thin films.

Doping percentage (at%)	Thickness, t (nm)	Resistance, R_S (MΩ)	Resistivity, ρ (Ω·cm)	Conductivity, σ (10^{-2} (Ω·m)$^{-1}$)	Carrier concentration, n (10^{17} cm^{-3})	Mobility, μ (cm^2/(V·s))
0	130	21.5	2.80	0.358	0.15	1.53
5	140	6	0.84	1.19	0.59	1.26
10	135	2	0.27	3.70	2.14	1.08
15	145	3.2	0.46	2.17	1.01	1.34
20	152	5.1	0.78	1.29	0.54	1.49

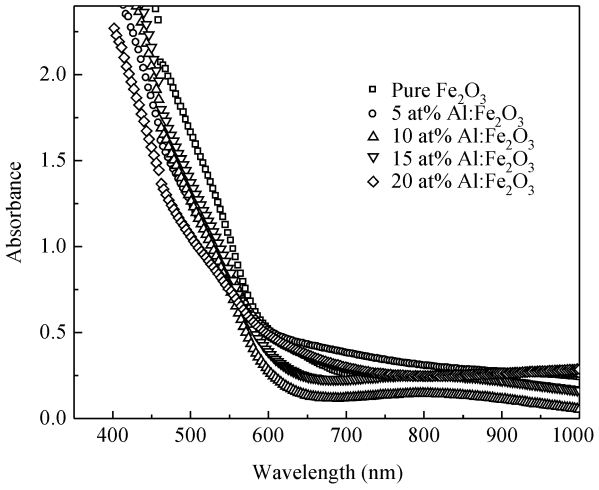

Fig. 4. Variation in absorbance (αt) versus wavelength (λ).

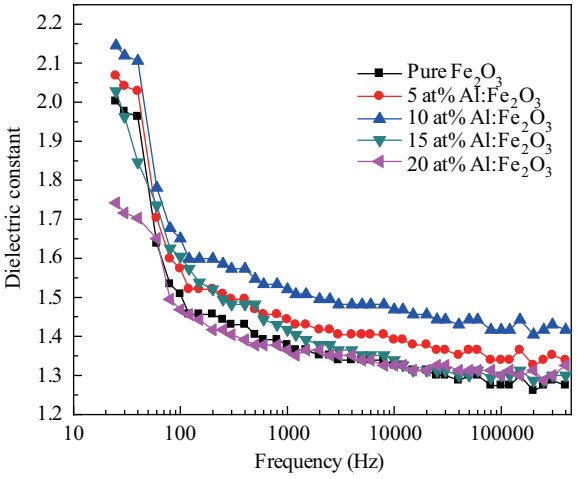

Fig. 5. Variation in room temperature dielectric constant with frequency.

fect might be enhanced due to scattering from a rough surface. The decrease in transmittance at higher doping concentrations may be due to the increased scattering of photons by crystal defects created by doping. The free carrier absorption of photons may also contribute to the reduction in optical transmittance[21]. In transparent metal oxides, the metal to oxygen ratio decides the percentage of transmittance. A metal rich film usually exhibits less transparency. The amplitude of the interference fringes decreased for higher doping concentration and this indicated a loss in surface smoothness leading to a slight scattering loss.

The variation in optical absorption with wavelength is shown in Fig. 4. The band edge of inorganic solid is located at the low energy end of the continuum band above the valence band. It is difficult to determine the band edge for transition metal oxides because there are a lot of narrow d–d bands in the gap, and some even extend into infrared region with a definite probability. It is widely accepted that the band edge of Fe_2O_3 is located in the range of 580–620 nm[22]. Clearly the transitions in this energy region include the d–d transition, pair excitation and less charge transfer, and the former two transitions mainly come from the narrow d bands, so the optical properties of the Fe_2O_3 band edge cannot be accounted for intrinsic semiconductor. The short photoexcited electron lifetime of Fe_2O_3 nano-clusters provides evidence for the fast relaxation of neighboring d levels[23]. The absorption spectrum exhibits a broad absorption in the visible region, with a tail extending up to 646 nm. The threshold of absorption at 564 nm (2.2 eV) is in approximate agreement with the bandgap value of 2.2 eV for undoped Fe_2O_3[24]. The optical band gap increases from 2.2 to 2.25 eV, with the aluminium doping concentration showing a slight blue shift due to degeneracy of the semiconductor. The indirect transition has been identified as a spin-forbidden Fe^{3+} 3d–3d excitation, while the direct transition corresponds to the $O^{2-}2p$–$Fe^{3+}3d$ charge transfer[25]. The band gap of doped thin films is greater than the single crystal value reflecting the nanocrystalline phase of the films.

3.4. Electrical and dielectric properties

The influence of aluminium doping concentration on the resistivity and conductivity of iron oxide thin films is shown in Table 1. Initially, the resistivity decreases with doping concentration up to 10 at% Al and then increases due to the fact that aluminium exceeds the limit of maximum solubility in iron oxide, producing a grain boundary segregation of impurities that causes a dispersion of carriers. The room temperature electrical resistivity is of the order of $\sim 10^2$ Ω·cm, which is much less than previously reported values for iron oxide thin films prepared by spray pyrolysis[26]. Table 1 depicts the nature of carrier concentration and mobility of Al:Fe_2O_3 thin films with respect to doping concentration for films (determined from Hall effect measurement). The carrier concentration increases with aluminium doping concentration, until it reaches a maximum value for 10 at% Al doping and then decreases. However, mobility decreases with Al doping, being at a minimum for 10 at% doping. Further increase in doping concentration leads to an increase in mobility due to an enhancement in grain size. Mobility variation is due to the dominant ion impurity scattering mechanism.

Due to increasing interest in the dielectric properties of ox-

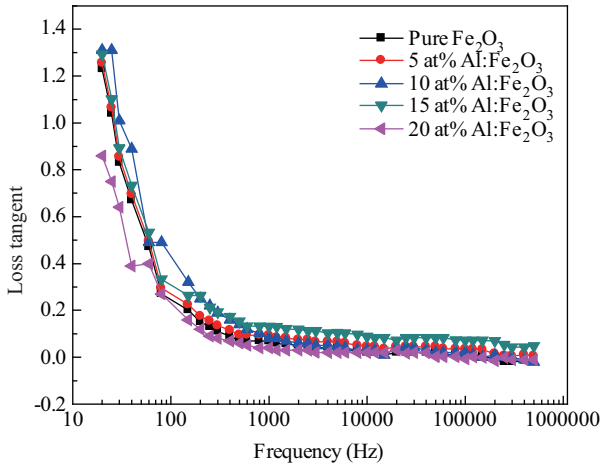

Fig. 6. Variation in loss tangent (tan δ) with frequency.

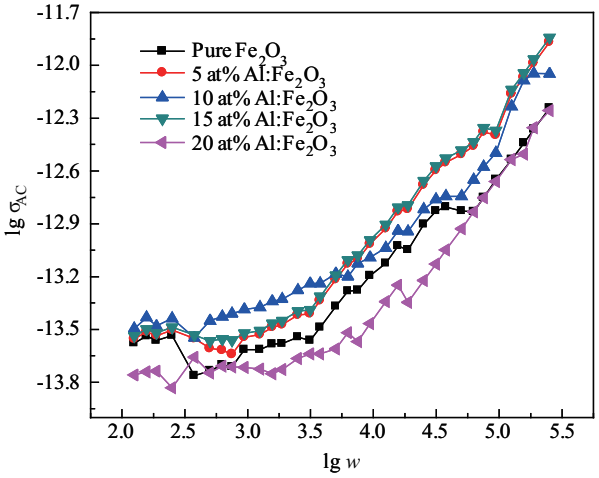

Fig. 7. Variation in AC conductivity with frequency.

ides, dielectric measurements of iron oxide thin film are carried out. The room temperature performance of the dielectric constant with frequency is shown in Fig. 5. From this figure, it is clear that the dielectric constant (ε') decreases abruptly at lower frequencies and remains constant at higher frequencies, showing the dispersion of dielectric constant at lower frequencies due to the charge transport relaxation time. The dielectric constant increases up to 10 at% doping and then it decreases. The large value of the dielectric constant (2.15 at 1000 Hz for 10 at% Al:Fe_2O_3) is associated with space charge polarization and inhomogeneous dielectric structure viz. impurities, grain structure, defects and pores. The decrease in dielectric constant takes place when jumping frequency of electric charge cannot follow the alternations of applied electric field beyond a certain critical frequency. This dielectric dispersion is attributed to the Maxwell[27] and Wagner[28] type of interfacial polarization in agreement with Koop's phenomenological theory[29]. Since polarization decreases with increasing frequency and reaches constant values, a decrease in dielectric constant with frequency is observed. At lower frequencies, dielectric loss tan δ (Fig. 6) is large and it decreases with increasing frequency. The tan δ is the energy dissipation in the dielectric system, which is proportional to the imaginary part of the dielectric constant. An increase in loss factor at higher frequencies may be due to the series resistance of the electrodes, leads, etc.[30]. The appearance of minimum loss with frequency is a direct consequence of a mathematical analysis of an equivalent capacitance circuit for oxide dielectric films[31]. The plots (Fig. 7) are observed to be almost linear, indicating that the AC conductivity (σ_{ac} proportional to angular frequency) increases with increase in frequency, confirming the small polaron mechanism of conduction. The higher values of dielectric constant, loss tangent and AC conductivity observed at 10 at% Al:Fe_2O_3 may be due to the large surface charge sorption of the Al^{3+} ion in Fe_2O_3 thin films as compared with other doping concentrations[32].

3.5. Thermal conductivity

The variation in specific heat and thermal conductivity with respect to the doping concentration is illustrated in Fig. 8.

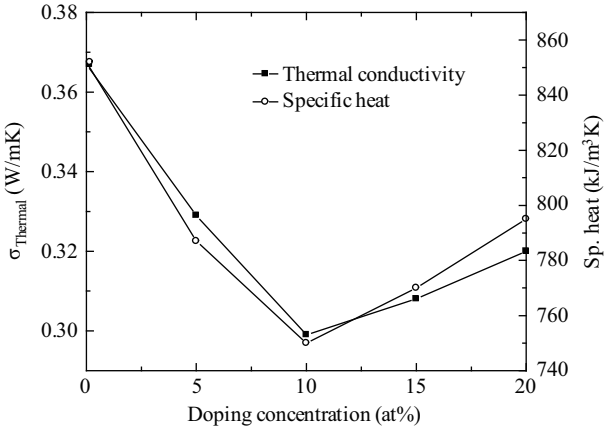

Fig. 8. Plot of thermal conductivity against aluminium doping percentage in Al:Fe_2O_3 thin films.

Specific heat and thermal conductivity decreases up to a 10 at% Al doping concentration (attains minimum value 750 kJ/m^3·K and 0.299 W/mK respectively) and then increases with higher doping concentrations. The decrease in thermal conductivity means that phonon conduction behavior is dominant in these polycrystalline films[29], while the increase in thermal conductivity for higher concentrations is mainly attributed to the significant change in microstructure. Apart from the contribution of the microstructure, the lower thermal conductivity of films can be attributed to intrinsic factors. The thermal conductivity of a crystalline solid is due to changes in lattice vibrations, which are usually described in terms of phonons.

3.6. Photoelectrochemical performance

In order to improve the photoelectrochemical performance, generally the following photoelectrode properties are desirable: (1) a photoelectrode that has a large surface area to increase the interfacial reaction sites, (2) an optically thicker and efficient photoelectrode to enable total absorption of solar light, (3) appropriate morphological features (size, shape, grain boundaries, interconnection of particles, defects, etc.) that de-

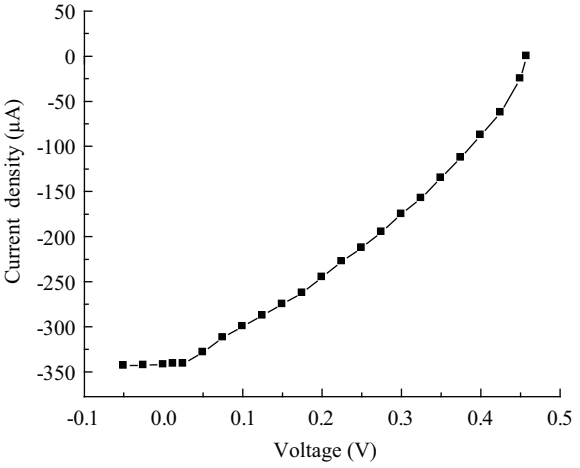

Fig. 9. Current–voltage characteristics for 10 at% AFO thin film under white light illumination in a NaOH electrolyte.

fine the energetics and kinetics at the electrode interface, and hence influence the PEC efficiency of the solar cell, and (4) an electrode comprising a densely packed array of grains, which can enhance PEC performance by virtue of the improvement in the carrier transport mechanism and minimizing surface trap states. The unique structure combining high crystallinity and large surface area leads to higher PEC performance. Recently, an improvement in the PEC properties of iron oxide electrodes by doping of various defects has been demonstrated[33, 34].

Figure 9 shows the photocurrent–voltage (I–V) plot for optimized 10 at% Al:Fe_2O_3 photoelectrodes under illumination of visible light. The unintentional incorporation of donor-type species may also be responsible for improving the photo efficiency. The Al doped Fe_2O_3 thin films exhibited a several times better photoresponse as compared with undoped (α-Fe_2O_3) films. A plausible explanation for the enhanced photoelectrochemical response could be related to the fact that Al doped iron oxide films are converted to a wide band gap and act as an efficient catalyst for swift migration of the photogenerated charge carriers. Also, the crystallographic orientation degree of the films appears to be a dominant factor affecting the photocurrent. The photoelectron collection was enhanced because of the orientation of the strongly conducting basal planes, whereas the photohole transfer was facilitated by the short diffusion distances from nanostructure to electrolyte. Under illumination, the current–voltage (I–V) characteristics of "FTO/Al:Fe_2O_3/electrolyte/SCE" cells are measured. From the above cell configuration it is seen that even in dark PEC cell gives some dark voltage V_d with Al:Fe_2O_3 thin film as the working electrode and graphite as the counter electrode. The origin of this voltage is attributed to the difference between the two half-cell potentials in the PEC cell. Upon illumination of the junction, the magnitude of the open circuit voltage increases with the negative polarity towards the Al:Fe_2O_3 photoanodes. Thus, the cathodic behavior of the photo-voltage of the semiconductor indicates that the Al:Fe_2O_3 electrode is of n-type. The n-type behavior is commonly observed due to the carrier concentration established by oxygen vacancies and excess iron sites[35]. These (I–V) curves in the dark indicate good junction rectification properties. After illumination, the shift of the I–V curve in the fourth quadrant reveals that the cell can work as a generator of electricity. Out of four electrolytes (Na_2SO_4, KOH, KI and NaOH), NaOH is a promising electrolyte for successful PEC manipulation. From the I–V measurements, it is observed that the higher magnitudes of I_{sc}, V_{oc}, the fill factor and the efficiency (341 μA, 458 mV, 0.38 and 2.37%, respectively) are obtained for the electrodes using a NaOH electrolyte. This behavior can be attributed to the fact that the NaOH electrolyte allows the sample to absorb more light photons than other electrolytes, viz. KI, KOH, Na_2SO_4. The fill factor value obtained in our experiments is quite close to that of solar cells based on iron oxide films. In conclusion, the improvement in the PEC properties of the doped thin films is due to (1) morphological modifications that enhance the active surface area and (2) quenching of the defect levels responsible for recombination losses, as compared to the pure hematite α-Fe_2O_3. This approach may pave the way to synthesize better doped iron oxide electrodes for PEC solar cells. The junction parameter can be obtained by using a simple diode equation,

$$I = I_0\left(\mathrm{e}^{eV/nkT} - 1\right), \tag{5}$$

where n is the junction ideality factor, I_0 the reverse saturation current, V the forward bias voltage, and I the forward current in the dark. The fill factor is calculated from

$$\mathrm{FF} = \frac{I_m V_m}{I_{sc} V_{oc}}, \tag{6}$$

where I_m and V_m are the values of maximum current and maximum voltage, which can be extracted from the PEC solar cell. The efficiency η (in %) is calculated from

$$\eta = \frac{V_{oc} I_{sc} \mathrm{FF}}{P_{input}} \times 100, \tag{7}$$

where P_{input} is the input light energy. R_S the series resistance and R_{Sh} the shunt resistance are estimated from slope of power output characteristics using

$$\left(\frac{\mathrm{d}I}{\mathrm{d}V}\right)_{I=0} = \frac{1}{R_S}, \tag{8}$$

$$\left(\frac{\mathrm{d}I}{\mathrm{d}V}\right)_{V=0} = \frac{1}{R_{Sh}}. \tag{9}$$

It is seen that there is an increase in V_{oc}, I_{sc}, η, FF, and R_{sh} and a decrease in the R_s after Al doping. Under visible illumination, the output characteristic parameters in terms of open circuit voltage (V_{oc}), short circuit current density (I_{sc}), power conversion efficiency, series and shunt resistance and fill factor (FF), etc with various electrolytes (KI, KOH, NaOH and Na_2SO_4) for pure and 10 at% Al:Fe_2O_3 are presented in Tables 2 and 3. This may be due to the improvement of crystallinity and/or grain size and the decrease in resistivity of the doped films.

Another important parameter of the semiconductor that can be derived from Mott–Schottky measurements is the flat band potential. Although the flat band potential depends on the exposed crystal plane and on the donor density inside the films. Figure 10 shows a Mott–Schottky (M–S) plot of an n-Al:Fe_2O_3/sodium hydroxide electrolyte/C system in dark for

Table 2. Power output parameters of pure α-Fe_2O_3 photoanodes for various electrolytes.

Sr. No.	Electrolyte	I_{sc} (μA/cm^2)	V_{oc} (mV)	Fill factor	Efficiency (%)
1	KOH	23	165	0.24	0.036
2	NaOH	56	182	0.32	0.15
3	KI	31	172	0.26	0.055
4	Na_2SO_4	15	139	0.32	0.027

Table 3. Power output parameters of 10 at% Al:Fe_2O_3 photoanodes for various electrolytes.

Sr. No.	Electrolyte	I_{sc} (μA/cm^2)	V_{oc} (mV)	Fill factor	Efficiency (%)
1	KOH	176	398	0.32	0.896
2	NaOH	341	458	0.38	2.37
3	KI	227	414	0.26	0.93
4	Na_2SO_4	61	273	0.22	0.15

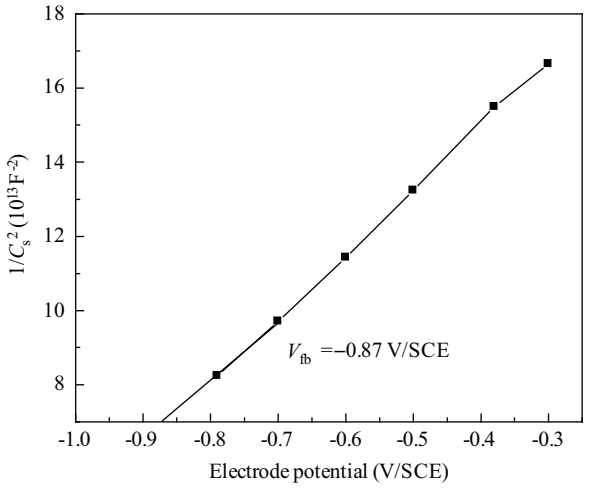

Fig. 10. Mott–Schottky measurement of 10 at% Al:Fe_2O_3 thin films for a NaOH electrolyte at frequency f = 100 Hz.

FTO-coated glass substrate-based PEC cell under reverse bias. The value of the flat band potential, V_{fb}, is obtained at $\frac{1}{C_S^2} = 0$ on the potential axis according to the well-known M–S relation[36, 37],

$$\left(\frac{1}{C_S^2}\right) = \frac{2}{\varepsilon_0 \varepsilon_s q N_D}\left(V - V_{fb} - \frac{kT}{q}\right), \qquad (10)$$

where C_S is the space charge capacitance. V_{fb} is found to be –0.87 V/SCE for AFO thin film.

4. Conclusions

We have presented an inclusive study of the interrelationship between the dopant concentration and physical properties of iron oxide thin films grown by pyrolytic decomposition in aqueous solution. In particular, we have investigated the influence of aluminium doping on the structural, morphological, optical, electric and dielectric properties with their photoelectrochemical performance. The α-Fe_2O_3 hematite phase with rhombohedral crystal structure in a hexagonal system is confirmed from the X-ray diffraction pattern. Doping of Al in Fe_2O_3 film shows a reduction in the particle size to quantum-size with delocalization of electrons, causing obvious blue-shifted and sharply increased optical absorption with an increase in band gap from 2.2 to 2.25 eV. Low mobility seen at optimized doping concentration confirms the increase in grain size and conductivity. The dielectric behavior shows the electronic polarizability at higher frequencies due to space charge polarization. AC conductivity increases with an increase in the frequency due to the hopping mechanism of conduction. Based upon the fundamental understanding of the factors governing the offset energies at electrolyte interfaces in the absence of a high density of background charge, we find that a power conversion efficiency approaching 2.37% is possible for 10 at% Al:Fe_2O_3 thin films with a flat band potential (V_{fb} = –0.87 V/SCE) in a NaOH electrolyte.

Acknowledgement

The authors are very much thankful to the University Grants Commission, New Delhi, through the UGC-DRS IInd phase Programme (2004-2009), and the Defense Research and Development Organization (DRDO), New Delhi, through its project ERIP/ER/0503504/M/01/007 for financial support.

References

[1] Aroutiounian V M, Arakelyan V M, Shahnazaryan G E, et al. Photoelectrochemistry of semiconductor electrodes made of solid solutions in the system Fe_2O_3–Nb_2O_5. Solar Energy, 2006, 80: 1098

[2] Ferretto L, Glisenti A. Study of the surface acidity of an hematite powder. J Mol Catal A: Chem, 2002, 187: 119

[3] Liu Y, Sun D. Effect of CeO_2 doping on catalytic activity of Fe_2O_3/γ-Al_2O_3 catalyst for catalytic wet peroxide oxidation of azo dyes. J Hazard Mater, 2007, 143: 448

[4] Fu H, Quan X, Zhao H. Photodegradation of γ-HCH by α-Fe_2O_3 and the influence of fulvic acid. J Photochem Photobiol Chem, 2005, 173: 143

[5] Goodenough J B. Metallic oxides. Pergamon Press Ltd, 1971

[6] Younsi Y, Aider M, Bouguelia A, et al. Visible light-induced hydrogen over $CuFeO_2$ via $S_2O_3^{2-}$ oxidation. Solar Energy, 2005, 78: 574

[7] Saadi S, Bouguelia A, Trari M. Photocatalytic hydrogen evolution over $CuCrO_2$. Solar Energy, 2006, 80: 272

[8] Boumaza S, Bouarab R, Trari M, et al. Hydrogen photo-evolution over the spinel $CuCr_2O_4$. Energy Convers Manage, 2009, 50: 62

[9] Gerisher H. Energy conversion with semiconductor electrodes. In: Seraphin B O, ed. Topics in applied physics, solid state physics aspects. Berlin Heidelberg, New York: Springer-Verlag, 1979

[10] Lindgren T, Wang H, Beermann N, et al. Aqueous photoelectrochemistry of hematite nanorod array. Sol Energy Mater Sol Cells, 2002, 71: 231

[11] Goodlet G, Faty S, Cardoso S, et al. The electronic properties of sputtered chromium and iron oxide films. Corros Sci, 2004, 46: 1479

[12] Glasscok J A, Barnes P R F, Plumb I C, et al. Structural, optical and electrical properties of undoped polycrystalline hematite thin films produced using filtered arc deposition. Thin Solid Films, 2008, 516: 1716

[13] Valenzuela M A, Bosch P, Jiménez-Bercerrill J, et al. Preparation, characterization and photocatalytic activity of ZnO, Fe_2O_3 and $ZnFe_2O_4$. J Photochem Photobiol A, 2002, 148: 177
[14] Aroutiounian V M, Arakelyan V M, Shahnazaryan G E, et al. Photoelectrochemistry of tin-doped iron oxide electrodes. Solar Energy, 2007, 81: 1369
[15] Shwarsctein A K, Huda M N, Walsh A, et al. Electrodeposited aluminum-doped α-Fe_2O_3 photoelectrodes: experiment and theory. Chem Mater, 2010, 22: 510
[16] Liang Y, Enache C S, Krol R. Photoelectrochemical characterization of sprayed α- Fe_2O_3 thin films: influence of Si doping and SnO_2 interfacial layer. International J Photoenergy, 2008, ID 739864
[17] Mathur S, Sivakov V, Shen H, et al. Nanostructured films of iron, tin and titanium oxides by chemical vapor deposition. Thin Solid Films, 2006, 502: 88
[18] Chatzitheodorou G, Fiechter S, Kfnenkamp R, et al. Thin photoactive FeS_2 (pyrite) films. Mater Res Bull, 1986, 21: 1484
[19] Birkholz M, Lichtenberger D, Hfpfner C, et al. Sputtering of thin pyrite films. Sol Energy Mater Sol Cells, 1992, 27: 243
[20] Sivako V, Petersen C, Daniel C, et al. Laser induced local and periodic phase transformations in iron oxide thin films obtained by chemical vapour deposition. Appl Surf Sci, 2005, 247: 513
[21] Kumar P M R, Kartha C S, Vijayakumar K P, et al. On the properties of indium doped ZnO thin films. Semicond Sci Technol, 2005, 20: 120
[22] Sherman D M, Waite T D. Electronic spectra of Fe^{3+} oxides and oxide hydroxides in the near IR to near UV. Am Mineral, 1985, 70: 1262
[23] Cherepy N J, Liston D B, Lovejoy J A, et al. Ultrafast studies of photoexcited electron dynamics in γ- and α-Fe_2O_3 semiconductor nanoparticles. J Phys Chem B, 1998, 102: 770
[24] Somorjai G A, Leygraf C H. Electrolytic photodissociation of chemical compounds by iron oxide photochemical diodes. US Patent, No. 4533608, 6 Aug 1985
[25] Duret A, Gratzel M. Visible light-induced water oxidation on mesoscopic α-Fe_2O_3 films made by ultrasonic spray pyrolysis. J Phys Chem B, 2005, 109: 17184
[26] Pawar S H, Patil P S, Madhale R D, et al. Preparative parameters and dependent properties of Fe_2O_3 films formed by spray pyrolysis technique. Indian J Pure Appl Phys, 1989, 27: 227
[27] Maxwell J C. Electricity and magnetism. London: Oxford University Press, 1993: 828
[28] Sawant V S, Shinde S S, Deokate R J, et al. Effect of calcining temperature on electrical and dielectric properties of cadmium stannate. Appl Surf Sci, 2009, 255: 6675
[29] Babar A R, Shinde S S, Moholkar A V, et al. Electrical and dielectric properties of co-precipitated nanocrystalline tin oxide. J Alloys Compd, 2010, 505: 743
[30] Goswami A, Goswami A P. Dielectric and optical properties of ZnS films. Thin Solid Films, 1973, 16: 175
[31] Pratt I H, Firestone S J. Fabrication of RF-sputtered barium titanate thin films. J Vac Sci Technol, 1971, 8: 256
[32] Janusz W, Sworska A, Szezypa J. Electrical double layer at the α-Fe_2O_3-mixed electrolyte (ethanol-aqueous) interface. J Colloids Surf A, 1999, 149: 421
[33] Ingler W B Jr, Khan S U M. Photoresponse of spray pyrolytically synthesized copper-doped p-Fe_2O_3 thin film electrodes in water splitting. International Journal of Hydrogen Energy, 2005, 30: 821
[34] Ingler W B Jr, Khan S U M. Photoresponse of spray pyrolytically synthesized magnesium-doped iron (III) oxide (p-Fe_2O_3) thin films under solar simulated light illumination. Thin Solid Films, 2004, 461: 301
[35] Miller E L, Paluselli D, Marsen B, et al. Low-temperature reactively sputtered iron oxide for thin film devices. Thin Solid Films, 2004, 466: 307
[36] Mott N F. The theory of crystal rectifiers. Proc R Soc A, 1939, 171: 27
[37] Sawant R R, Shinde S S, Bhosale C H, et al. Influence of substrates on photoelectrochemical performance of sprayed n-$CdIn_2S_4$ electrodes. Solar Energy, 2010, 84: 1208